JOURNAL OF VIROLOGY, June 2004, p. 6469–6479 Vol. 78, No. 12
0022-538X/04/$08.00+0 DOI: 10.1128/JVI.78.12.6469–6479.2004

Inter- and Intragenus Structural Variations in Caliciviruses and Their Functional Implications

Rong Chen,[1] John D. Neill,[2] Jacqueline S. Noel,[3] Anne M. Hutson,[4] Roger I. Glass,[3] Mary K. Estes,[4] and B. V. Venkataram Prasad[1]*

Verna and Marrs McLean Department of Biochemistry and Molecular Biology[1] and Department of Molecular Virology and Microbiology,[4] Baylor College of Medicine, Houston, Texas 77030; National Animal Disease Center, Agriculture Research Service, U.S. Department of Agriculture, Ames, Iowa 50010[2]; and Viral Gastroenteritis Unit, Division of Viral and Rickettsial Diseases, National Center for Infectious Diseases, Centers for Disease Control and Prevention, Atlanta, Georgia 30333[3]

Received 9 September 2003/Accepted 5 February 2004

The family *Caliciviridae* is divided into four genera and consists of single-stranded RNA viruses with hosts ranging from humans to a wide variety of animals. Human caliciviruses are the major cause of outbreaks of acute nonbacterial gastroenteritis, whereas animal caliciviruses cause various host-dependent illnesses with a documented potential for zoonoses. To investigate inter- and intragenus structural variations and to provide a better understanding of the structural basis of host specificity and strain diversity, we performed structural studies of the recombinant capsid of Grimsby virus, the recombinant capsid of Parkville virus, and San Miguel sea lion virus serotype 4 (SMSV4), which are representative of the genera *Norovirus* (genogroup 2), *Sapovirus*, and *Vesivirus*, respectively. A comparative analysis of these structures was performed with that of the recombinant capsid of Norwalk virus, a prototype member of *Norovirus* genogroup 1. Although these capsids share a common architectural framework of 90 dimers of the capsid protein arranged on a T=3 icosahedral lattice with a modular domain organization of the subunit consisting of a shell (S) domain and a protrusion (P) domain, they exhibit distinct differences. The distally located P2 subdomain of P shows the most prominent differences both in shape and in size, in accordance with the observed sequence variability. Another major difference is in the relative orientation between the S and P domains, particularly between those of noroviruses and other caliciviruses. Despite being a human pathogen, the Parkville virus capsid shows more structural similarity to SMSV4, an animal calicivirus, suggesting a closer relationship between sapoviruses and animal caliciviruses. These comparative structural studies of caliciviruses provide a functional rationale for the unique modular domain organization of the capsid protein with an embedded flexibility reminiscent of an antibody structure. The highly conserved S domain functions to provide an icosahedral scaffold; the hypervariable P2 subdomain may function as a replaceable module to confer host specificity and strain diversity; and the P1 subdomain, located between S and P2, provides additional fine-tuning to position the P2 subdomain.

The *Caliciviridae*, a family of nonenveloped, icosahedral, positive-sense, single-stranded RNA viruses, is divided into four genera, *Norovirus*, *Sapovirus*, *Lagovirus*, and *Vesivirus* (16). In this classification, which is based on genome organization and sequence comparisons, all human caliciviruses are grouped within the first two genera and most animal caliciviruses are grouped within the other two genera. Human caliciviruses are the major cause of epidemic nonbacterial gastroenteritis, whereas the animal caliciviruses cause a variety of host-dependent diseases (14, 17). The study of human caliciviruses has been hampered by the lack of either cell culture or animal model systems that support the propagation of these caliciviruses (16, 17). Recombinant empty capsids of several human caliciviruses have been produced from baculovirus-expressed capsid proteins (2, 11, 18, 22, 26, 27, 30, 34, 43), and these recombinant capsids have been shown to be morphologically and antigenically similar to authentic virions (27). Much of our understanding of these human caliciviruses, in terms of their molecular biology, structure, and immunology, has been obtained through the study of these recombinant capsids (17, 29).

Unlike human caliciviruses, which are resistant to in vitro cultivation, some animal caliciviruses, including primate calicivirus (54), feline calicivirus (36), and San Miguel sea lion virus (SMSV) (50), have been successfully propagated in cell culture. These viruses have provided a direct approach for the study of virus infections, genome transcription, viral protein translation, and virus replication (19, 59). Recent studies have indicated that some animal caliciviruses are capable of crossing species barriers and potentially use humans as their hosts. One serotype of SMSV was reported to infect humans (51, 53). The zoonotic potential of feline calicivirus has been suggested by the observation of a human antibody against it (53). More recently, the potential existence of animal reservoirs and the possibility of interspecies transmission have been suggested by the phylogenetic relatedness and classification of bovine and porcine viruses, isolated from the enteric tracts or fecal specimens of infected animals, within the genera *Norovirus* and *Sapovirus*, respectively (6, 9, 20, 35, 49, 57, 60).

Three-dimensional structures of a primate calicivirus (genus *Vesivirus*) and the recombinant capsid of the rabbit hemor-

* Corresponding author. Mailing address: Verna and Marrs McLean Department of Biochemistry and Molecular Biology, Alkek Building N410, Baylor College of Medicine, One Baylor Plaza, Houston, TX 77030. Phone: (713) 798-5686. Fax: (713) 798-1625. E-mail: vprasad@bcm.tmc.edu.

rhagic disease virus (genus *Lagovirus*) have been determined by electron cryomicroscopy (cryo-EM) to a resolution of ~22 Å (45, 58). The only high-resolution structure of a calicivirus is that of the recombinant capsid of Norwalk virus (NV) determined by X-ray crystallography (44). The structural studies showed that caliciviruses contain a T=3 icosahedral capsid composed of 180 capsid protein molecules organized into 90 dimeric capsomeres. The X-ray crystallographic studies revealed that the capsid protein has the following two principal domains: a shell (S) domain, with a typical eight-stranded β-barrel fold that is commonly seen in other viral capsid proteins (47), and a protrusion (P) domain that can be further divided into two subdomains called P1 and P2. The distally located P2 subdomain is a large insertion in the P1 subdomain. A comparison of the capsid proteins from various caliciviruses reveals significant variations both in their sequences and in their sizes. Although the S domain is well conserved, the P1 subdomain is only moderately conserved and the P2 subdomain is highly variable in these viruses (13). In general, the capsid proteins of human caliciviruses are smaller than those of animal caliciviruses.

Here we report a comparative cryo-EM analysis of representative caliciviruses from three different genera. Structural differences and similarities between the different caliciviruses were analyzed in the light of the available sequence data and the X-ray crystallographic structure of recombinant NV (rNV) to examine how the sequence variations and capsid sizes affect the structure and to gain insight into the basis of host specificity and strain diversity. The caliciviruses used for this study, namely the recombinant capsids of NV (genus *Norovirus*), Grimsby virus (GrV; genus *Norovirus*) (22), and Parkville virus (PV; genus *Sapovirus*) (42) and SMSV serotype 4 (SMSV4; genus *Vesivirus*) (40), were chosen to allow us to examine possible structural variations within a genus, across different genera, and between recombinant empty capsids and virions containing an intact genome. NV and GrV were chosen as representative examples of human caliciviruses within the same genus but belonging to different genogroups. The capsid protein of GrV (539 residues) exhibits 43% sequence identity with that of NV (530 residues) (17). PV, a human calicivirus, was chosen as a prototype example from the genus *Sapovirus* (42). One difference between noroviruses and sapoviruses is in their genome organization. In contrast to three open reading frames (ORFs) in noroviruses, sapoviruses contain two ORFs in their genomes. The PV capsid protein (571 residues) exhibits only 20% sequence identity with that of NV (16). Our studies of recombinant PV (rPV) reported here indeed represent the first structural characterization of a sapovirus. SMSV4, together with a primate calicivirus, belongs to the genus *Vesivirus*, a group of animal caliciviruses (16). The members of this genus have a broad host range and cause a variety of illnesses. Marine mammals such as pinnipeds and cetaceans are the natural hosts of SMSV, and infections can lead to abortions and vesicular lesions (50, 52, 55), whereas the primate calicivirus was originally isolated from a pygmy chimpanzee (54). At least 16 serotypes of SMSV have been identified, of which serotypes 1 and 4 have been further characterized (40). One serotype of SMSV has a list of several natural hosts that includes seals, cattle, whales, donkeys, and humans (51). A unique feature of vesiviruses is that the capsid protein present in the mature virion is a cleaved product of the capsid protein precursor encoded by the second ORF (5, 15, 56). In SMSV4, the mature 65-kDa capsid protein is proteolytically processed from the 78-kDa capsid protein precursor (15).

MATERIALS AND METHODS

Purification of rGrV capsids. The GrV capsid protein was expressed and the self-assembled virus-like particles were purified by previously described methods (22). Briefly, spinner flasks containing 3.5×10^6 Sf9 insect cells per 200 ml of Grace's insect cell medium were infected with the pFastBac-1/GrV ORF2 recombinant baculovirus at a multiplicity of infection of 5. At 7 days postinfection, the recombinant GrV (rGrV) capsids were harvested from the supernatants of spinner flask cultures, and the cells were pelleted and discarded. The capsids in the supernatant were pelleted by ultracentrifugation through a 30% sucrose cushion made with 0.2 M phosphate-buffered saline for virus-like particles (PBS-V; 0.2 M sodium phosphate, 1.0 M NaCl, pH 6.0) in an SW28 rotor at 120,000 × *g* for 3 h at 4°C. The pellets were suspended in 0.37 g of CsCl (Invitrogen, Grand Island, N.Y.) per ml of PBS-V and subjected to isopycnic gradient centrifugation in an SW55 rotor at 150,000 × *g* for 18 to 24 h at 4°C. The visible band of the rGrV capsids in the CsCl gradient was collected by use of a micropipette. CsCl was removed by diluting the capsids in PBS-V and sedimenting them by ultracentrifugation in an SW28 rotor at 120,000 × *g* for 3 h at 4°C. The capsid pellet was suspended in PBS-V, overlaid onto a 10 to 60% sucrose gradient, and separated by velocity sedimentation in an SW41 rotor at 100,000 × *g* for 40 min at 4°C. The band of rGrV capsids in the sucrose gradient was collected by use of a micropipette, diluted in PBS-V, and sedimented by ultracentrifugation in an SW28 rotor at 120,000 × *g* for 3 h at 4°C. The pellet was suspended in PBS-V containing protease inhibitors (1 μg each of aprotinin, leupeptin, and pepstatin/ml [Sigma, St. Louis, Mo.]) and stored at 4°C. The rGrV capsids were dialyzed against PBS before cryo-EM experiments.

Expression and purification of rPV capsids. A PCR fragment (nucleotides 793 to 2521) comprising ORF2 (nucleotides 793 to 2505) and ORF3 (nucleotides 2504 to 2521) of PV (U73124) was amplified by using primers PV2 (CTAG**TC TAGA**ATGGAGGGCAATGGCTCCAAATTG) and PV3 (ATAAGAAT**GCG GCCGC**CAACTAACCAACTCATTGGAA). The resulting amplicon was digested, ligated into the transfer vector pVL1393 (Pharmingen, San Diego, Calif.) at restriction sites XbaI and NotI, which were engineered into primers PV2 and PV3, respectively (shown in bold above), and transformed into HB101 cells. Positive clones were selected based on their nucleotide sequence. The production of recombinant baculoviruses and purification of recombinant capsids were performed as described by Belliot et al. (2).

Purification of SMSV4 virions. SMSV4 was propagated and purified as described previously (41). Briefly, Vero cells were maintained in Eagle's minimal essential medium supplemented with 0.25% lactalbumin hydrolysate and 10% fetal bovine serum. SMSV4 was propagated by infecting Vero cells at 37°C. The medium was harvested after the cytopathic effect was complete (at 24 h postinfection), followed by one cycle of freezing and thawing. Virions were precipitated by the addition of solid polyethylene glycol 8000 to a concentration of 10% (vol/vol), suspended in PBS (pH 7.6), and separated out by ultracentrifugation in a CsCl step gradient. The viral band was removed from this gradient and resedimented in a CsCl isopycnic gradient. The viral band was removed, diluted in PBS, and pelleted by ultracentrifugation. The virus pellet was suspended in PBS overnight at 4°C.

Cryo-EM. Samples for cryo-EM were each embedded in a thin layer of vitreous ice on holey carbon films by standard procedures (12). Frozen hydrated specimens were imaged in a JEOL 1200 electron cryomicroscope using a 100-kV electron beam with a dose of ~10 $e^-/Å^2$ at a nominal magnification of ×40,000. For each specimen area, a focal pair was recorded, with the first one at a defocus length of ~1 μm and the second one at a defocus length of ~2 μm. Images were recorded on Kodak SO-163 electron films, with a 1-s exposure for each. Micrographs were developed for 12 min in Kodak D-19 developer and fixed for 10 min in Kodak fixer at 21°C.

3D structural analysis. Micrographs were chosen for structural analysis based on the criteria of ice quality, particle concentration, and optimum defocusing. Images were digitized with a Zeiss SCA1 microdensitometer (Carl Zeiss Inc., Englewood, Colo.) using a 7-μm step size. Pixels were then averaged to give a step size of 14 μm, which corresponded to 3.5 Å per pixel in the object. Particle images from digitized micrographs were boxed into individual particle images with a pixel area of 150 by 150. The determination of orientation parameters, their refinement, and three-dimensional (3D) reconstructions were performed with the ICOS Toolkit software suite (33). Orientations of the particles were

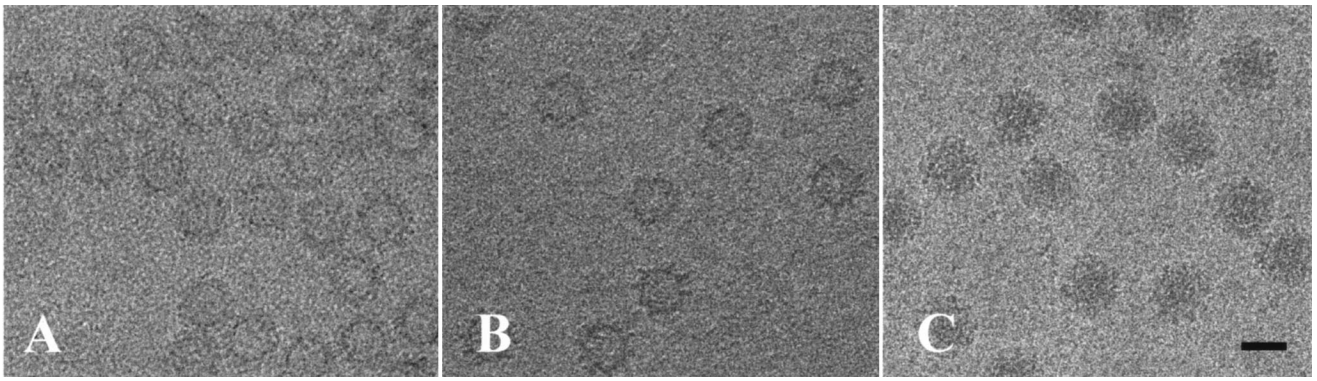

FIG. 1. Cryo-EM images of rGrV (A), rPV (B), and SMSV4 (C) particles embedded in vitreous ice. SMSV4 virions are substantially darker in the middle than the recombinant capsids (A and B) due to the presence of the RNA genome. Bar = 400 Å.

determined by the common lines method (7) and refined by cross-common lines procedures as described previously (33). 3D reconstructions were computed by cylindrical expansion methods (7). The final reconstructions were computed to a resolution that contained information within the first zero of the contrast transfer function (CTF) of the corresponding micrograph. The defocus value was determined from the CTF ring positions in the sum of particle Fourier transforms. Corrections for CTF were performed as described previously (63). The effective resolution of each reconstruction was estimated by using Fourier cross-correlation coefficients and equation 3 from the work of van Heel (61), and phase residuals were estimated by using equation 6 between independent reconstructions of the same specimen or between two independent reconstructions obtained by randomly dividing the data from a single micrograph into two subsets. The reconstructions were visualized on a Silicon Graphics workstation, using IRIS Explorer (NAG, Inc.) in conjunction with several customized modules (33). For each structure, the contour level was chosen to account for approximately 180 molecules of the corresponding capsid protein in the S and P domains. Radial density plots were computed from the 3D density maps by averaging the densities in concentric shells with a width of 3.5 Å about the center of the map.

Multiple sequence alignment and similarity plot. A total of 30 sequences of the capsid proteins or protein precursors of caliciviruses were obtained from the National Center for Biotechnology Institute's web site (http://www.ncbi.nlm.nih.gov/entrez). The data used were obtained from GenBank sequences M87661 (NV), AAA59233 (Oth25), U22498 (Mexico), AJ004864 (GrV), AAA18930 (Toronto), AAB00437 (Auckland), L23831 (Snow Mountain), U07611 (Hawaii), X86557 (Lordsdale), CAA54134 (Bristol), L07618 (Southampton), AB042808 (Chiba), AAC64603 (BS5), L23828 (KY89), U04469 (Desert Shield virus), AJ011099 (bovine), AF181082 (vesicular exanthema of swine virus), M87482 (SMSV4), AF091736 (Pan-1), M87481 (SMSV1), M86379 (FCV-F9), U13992 (FCV-CFI), D31836 (FCV-F4), U65427 (Sapporo), X86560 (Manchester), U73124 (PV), AF182760 (porcine), M67473 (rabbit hemorrhagic disease virus), Z69620 (European brown hare syndrome virus), and AB070225 (canine). A multiple sequence alignment was created by using the program CLUSTALW (http://clustalw.genome.ad.jp). For clarity, only 8 sequences, 2 from each genus, are shown in the sequence alignment plot, but the positions of all of the residues were derived from the alignment obtained for the 30 sequences. The S domain is not shown in the alignment because of its high similarity among all caliciviruses. Secondary structure predictions were carried out by using the program PHD (http://cubic.bioc.columbia.edu/predictprotein).

Fitting the X-ray structure of rNV into cryo-EM density maps. The X-ray structure of the rNV capsid protein (1IHM) and various cryo-EM density maps were visualized by using the program O (28) on an SGI workstation. The structure factors corresponding to cryo-EM density maps of various caliciviruses were calculated with the CCP4 software package (1). The S domain (residues 50 to 225), the P1 subdomain (residues 226 to 278 and 406 to 520), and the P2 subdomain (residues 279 to 405) were each treated as a fixed group for rigid body refinement with strict icosahedral symmetry imposed by the XPLOR software package (4). For rPV and SMSV4, manual fitting of both the P1 and P2 subdomains was performed with O before the rigid body refinement. The quality of fitting was judged by both visual inspection and R-factor calculations.

RESULTS

Electron cryomicrographs of empty particles and intact virions. Digitized electron cryomicrographs of the rGrV and rPV capsids and SMSV4 virions, each embedded in a thin layer of vitreous ice and recorded with about 1 μm of underfocus, are shown in Fig. 1. The rGrV and rPV capsids are both empty spherical shells with rough outer surfaces, consistent with the observation that the RNA genome is absent from these recombinant capsids. In some images, protrusions emanating from the spherical shell can be clearly seen. The images of SMSV4 virions are quite distinct from those of recombinant capsids. SMSV4 virions also contain a spherical shell with a rough outer surface. However, they appear substantially darker within the spherical shell due to the presence of the intact RNA genome.

3D reconstruction. The digitized micrographs for rGrV, rPV, and SMSV4 were each processed for image reconstruction. A total of 140, 105, and 241 particle images were included in the final reconstruction for rGrV, rPV, and SMSV4 (Fig. 2), respectively. CTF corrections were performed as described in Materials and Methods. In each case, the distribution of particle orientations covering the asymmetrical unit was sufficient for the resolution (22 Å) attained in the reconstruction, as at least 98% of the mean inverse eigenvalue spectrum was <0.01 (8). The resolution was confirmed by Fourier ring correlation analysis (61).

Calicivirus capsids share similar architectural features. Surface representations of the cryo-EM structures of rGrV, rPV, and SMSV4 along with that of the previously published cryo-EM structure of rNV at a similar resolution of ~22 Å are shown in Fig. 2. Despite noticeable differences in the surface morphology, all of these structures exhibited similar general features. The capsids of these viruses conform to T=3 icosahedral symmetry with 90 dimeric arch-like capsomeres at all the local and strict twofold axes of the T=3 lattice. These capsomeres are positioned in such a way that there are large hollows at all the icosahedral five- and threefold axes. The 180 subunits of the capsid protein can be classified into three quasi-equivalent subunits (A, B, and C; see Fig. 4) based on their locations on the T=3 icosahedral lattice. The dimers on the local twofold axes are formed by A and B subunits, whereas those on the strict twofold axes are formed by two C subunits.

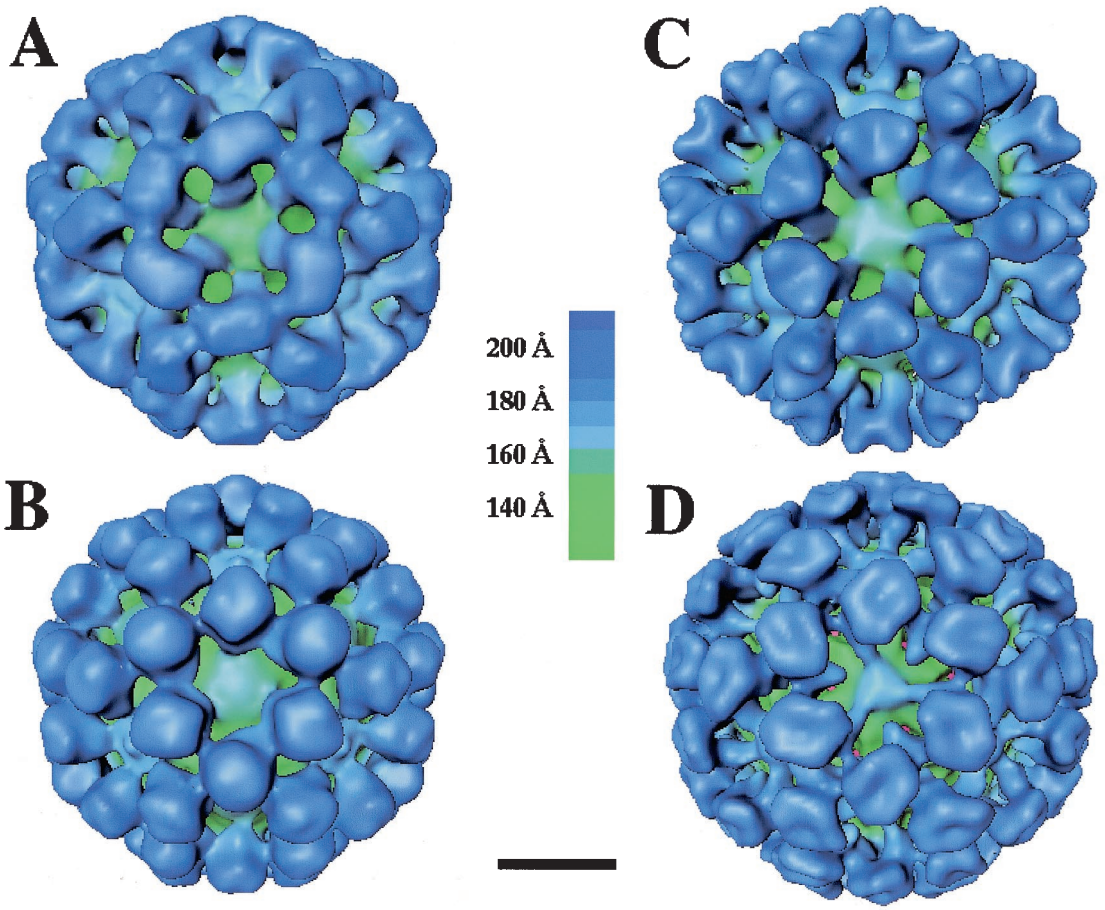

FIG. 2. Surface representations of the structures of rNV (A), rGrV (B), rPV (C), and SMSV4 (D) at a resolution of ~22 Å viewed along the icosahedral threefold axis. Structures are radially color coded according to the chart shown in the middle. Bar = 100 Å.

The AB dimers surround the icosahedral fivefold axes, whereas the AB and CC dimers alternate around the icosahedral threefold axes. Consistent with the X-ray structure of the rNV capsid, the capsid proteins of these viruses are also composed of two principal domains, the S and P domains. The S domains are involved in the formation of the contiguous icosahedral shell. The P domain is further divided into two subdomains: they are P1, which forms the leg of the arch, and P2, which forms the distal globular portion of the arch. The P2 subdomains of the opposing subunits in each dimer interact to form the top of the arch. These viruses exhibit significant variations in the shapes of the P2 subdomain as seen from the tops of the arches.

Radial density plots. Radial density profiles displaying the mass density distribution as a function of the radius from the center of the virus particle were computed for all of the reconstructions (Fig. 3). Beyond the radius of 110 Å, the radial density profiles of all the capsids matched well with the density profile of the rNV capsid, with two peaks corresponding to the S and P domains. In all of the structures, the icosahedral shell formed by the S domain lies between radii of 110 and 150 Å. Beyond the radius of 150 Å, one or two peaks due to the protruding P domain are seen in the radial density plots. In the structures of the rNV and rGrV capsids, the P domain lies between the radii of 150 and 190 Å, whereas in the structures of the rPV capsid and SMSV4, the P domain extends further, to a radius of ~200 Å. Based on the radial density plot analysis, it appears that the rPV capsid and SMSV4 have a slightly larger P domain than the rNV and rGrV capsids.

In the recombinant capsids (rNV, rPV, and rGrV), there is no significant density within the radius of 110 Å. However, SMSV4, a native calicivirus with an intact RNA genome, contains a significant amount of mass density within the icosahedral shell, and this density contributes to several additional peaks within the radius of 110 Å in the radial density plot (Fig. 3). Immediately within the radius of 110 Å, there is a distinct peak between the radii of 85 and 105 Å which corresponds to a contiguous shell in the structure. The composition of this inner contiguous shell, designated IS, is not clearly known (see Discussion). Further inside the IS, the mass density is likely due entirely to the RNA genome.

Structural variations in the P2 subdomain. The P2 subdomain, located at the top of the arches, is the most external part of the capsid protein. When different reconstructions are compared, the most noticeable differences are seen in this region. The rNV capsid has a rectangular platform at the top of the arches, whereas the rGrV capsid has a more rounded, globular shape (Fig. 4, top row). The rPV capsid has a saddle-shaped structure located on its top, and SMSV4 exhibits a rather parallelogram-shaped platform with a dent at the center.

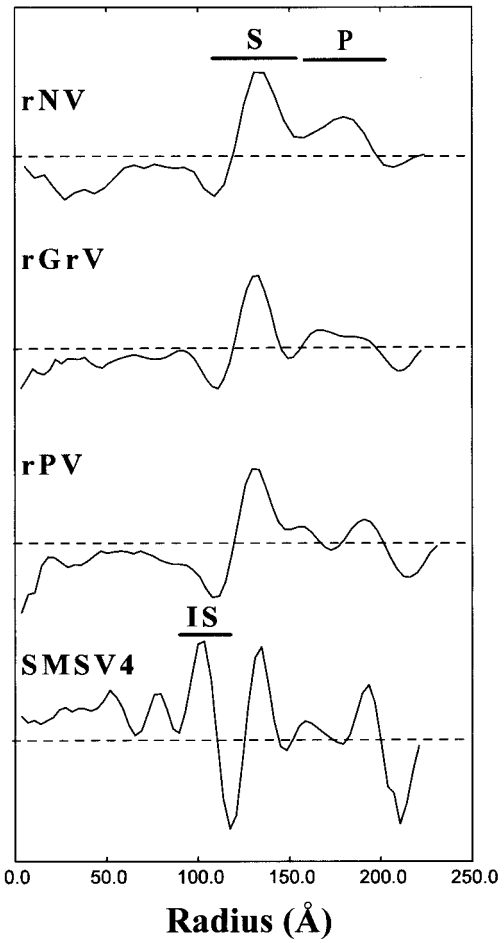

FIG. 3. Radial density plots of rNV, rGrV, rPV, and SMSV4 computed from their respective cryo-EM density maps. The dashed horizontal lines represent an average radial density of zero. The radial locations of the S and P domains as well as the IS are denoted.

Dimeric interactions of the P1 subdomain. The P1 subdomain is the connecting region between the S domain and the P2 subdomain. The rNV and rGrV capsids share a similar dimeric interaction pattern in this region which is distinct from that seen for rPV and SMSV4 (Fig. 4, bottom row). In the structures of rNV and rGrV, both the P1 and P2 subdomains appear to participate in the intradimeric interactions (Fig. 4). In contrast, in the rPV and SMSV4 structures, only the P2 subdomain is involved in intradimeric interactions, whereas the P1 subdomains of these capsids show connections between the neighboring A and C subunits, suggesting that this subdomain is involved in interdimeric interactions instead of the intradimeric interactions seen with rNV and rGrV. In the structures of rNV and rGrV, the P2 subdomain is rotated about 45° away from the P1 subdomain (Fig. 4, first two columns). In the rPV and SMSV4 structures, the change in the orientation between the respective P1 and P2 subdomains is relatively small (Fig. 4, last two columns).

Internal structural features in SMSV4. SMSV4, as a native virion, shows distinct structural features at inner radii (Fig. 5). Immediately underneath the shell between the 110- and 150-Å radii (shown in green in Fig. 5A), SMSV4 has another contiguous shell, which extends from a radius of 85 Å to a radius of 105 Å (shown in yellow in Fig. 5A). At a slightly lower contour level, 60 density connections are seen between these two shells (Fig. 5B, green areas). Within the radius of 85 Å, the density distribution changes from a featureless contiguous shell to a truncated dodecahedral structure with a plug-like mass density at each fivefold axis (Fig. 5C). It is likely that the RNA genome contributes predominantly to this part of the structure.

Sequence alignment and similarity plot. We took 30 sequences of either the capsid protein or the capsid protein precursor of caliciviruses from all four genera and performed a multiple sequence alignment using the program ClustalW. For clarity, only eight sequences (two sequences from each genus) are shown in the alignment plot (Fig. 6). Our alignment revealed that the amino acid sequences in the S domains are highly conserved among all caliciviruses, as was shown previously (13); therefore, only the P domains are shown in the alignment plot (Fig. 6). Although the exact boundary between the P1 and P2 subdomains (highlighted in orange and green, respectively, for the NV capsid protein in Fig. 6) in other capsid proteins is not yet known, we can clearly see that residues in the P1 region are more conserved than those in the P2 region. Furthermore, in different caliciviruses the residues in the P1 subdomain are roughly equal in number, whereas there is a large variation in the numbers of residues that make up the P2 subdomain. For example, GrV contains about 15 more residues in the P2 subdomain than does NV, and two other caliciviruses, PV and SMSV4, contain 45 and 50 more residues, respectively. The capsid protein of PV contains at least three prominent insertions located in the vicinity of residues 290 to 300, 360 to 370, and 380 to 390 in the NV capsid protein sequence. The capsid protein of SMSV4 contains at least four prominent insertions in the P2 subdomain compared to the NV capsid protein sequence (shown as four stretches of inverted triangles above the NV capsid protein sequence in Fig. 6).

Secondary structure predictions for the capsid proteins of GrV and PV and the capsid protein precursor of SMSV4 were done by using the program PHD. The secondary structure prediction for the NV capsid protein showed a good match with the secondary structure derived from the X-ray structure of the rNV capsid, which confirms the reliability of these predictions. The P domains of the capsid protein in GrV, PV, and SMSV4, as predicted, were all mainly composed of β-sheets and loops, similar to what was seen in the structure of the rNV capsid protein (Fig. 6). Interestingly, an α-helix was predicted to be present in the P1 subdomains of GrV, PV, and SMSV4, and its predicted position corresponds to the position where an α-helix is seen in the rNV structure (residues 439 to 448) (Fig. 6). In addition, some β-strands which are predicted to be located in the P1 subdomains of GrV, PV, and SMSV4 appear to occupy similar locations as the corresponding β-strands in rNV. Therefore, in the P1 subdomain, in addition to the moderate conservation of the primary sequences, the secondary structure also appears to be fairly well conserved.

Fitting the rNV crystal structure into cryo-EM density maps. The X-ray structure of the rNV capsid protein, the only high-resolution structure for a calicivirus, was used to analyze the structural differences and similarities in cryo-EM density maps. In this analysis, because of the possible changes in relative orientations between the S and P domains and also be-

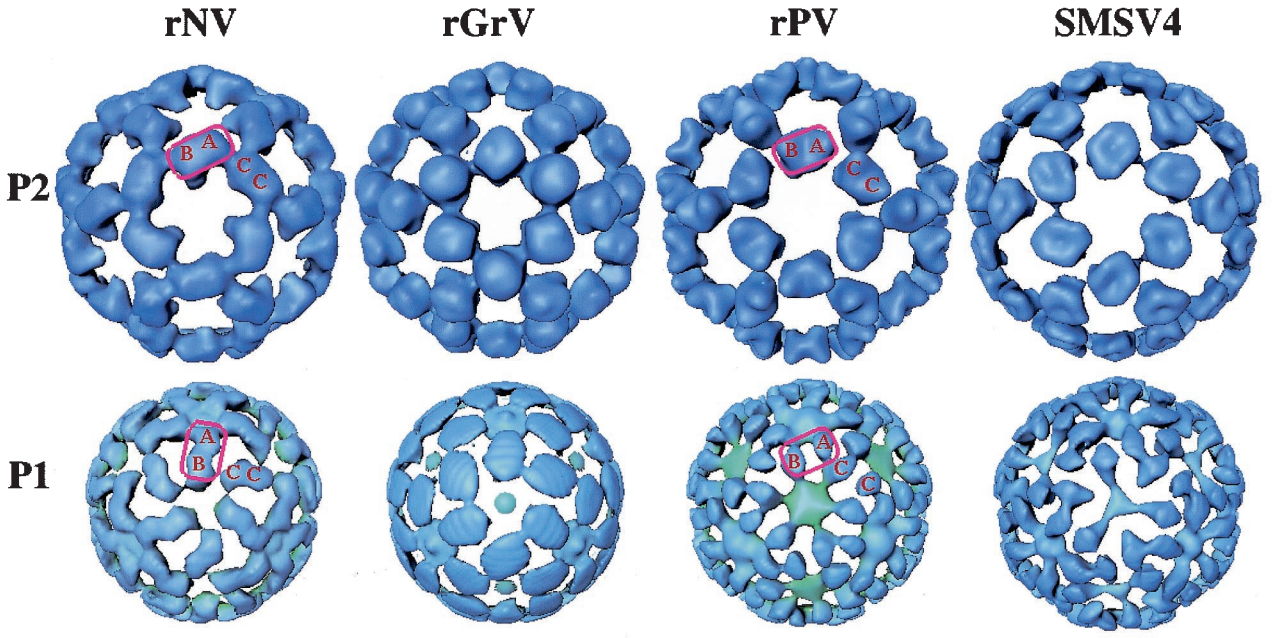

FIG. 4. Structural comparisons of the P1 and P2 subdomains among different caliciviruses. All of the surface representations are radially colored and viewed in the same orientation as in Fig. 2. The locations of the A, B, and C subunits are denoted. In the structures of rNV and rGrV, the P1 subdomain participates in intradimeric interactions, whereas in the structures of rPV and SMSV4, the same region is involved in interdimeric interactions. In rNV and rGrV, the P domain, shown inside a rectangular box, undergoes a twist of about 45° (compare the upper and lower panels), whereas in rPV and SMSV4, such a twist is not present.

tween the P1 and P2 subdomains, the S, P1, and P2 domains, each treated as an independent rigid body, were manually fitted into the corresponding regions in the cryo-EM density maps and subsequently subjected to rigid body refinement. During the fitting, we used additional constraints derived from the X-ray structure of the rNV capsid. In the rNV structure, the C terminus of the A subunit points towards the icosahedral fivefold axis, whereas those of the B and C subunits point

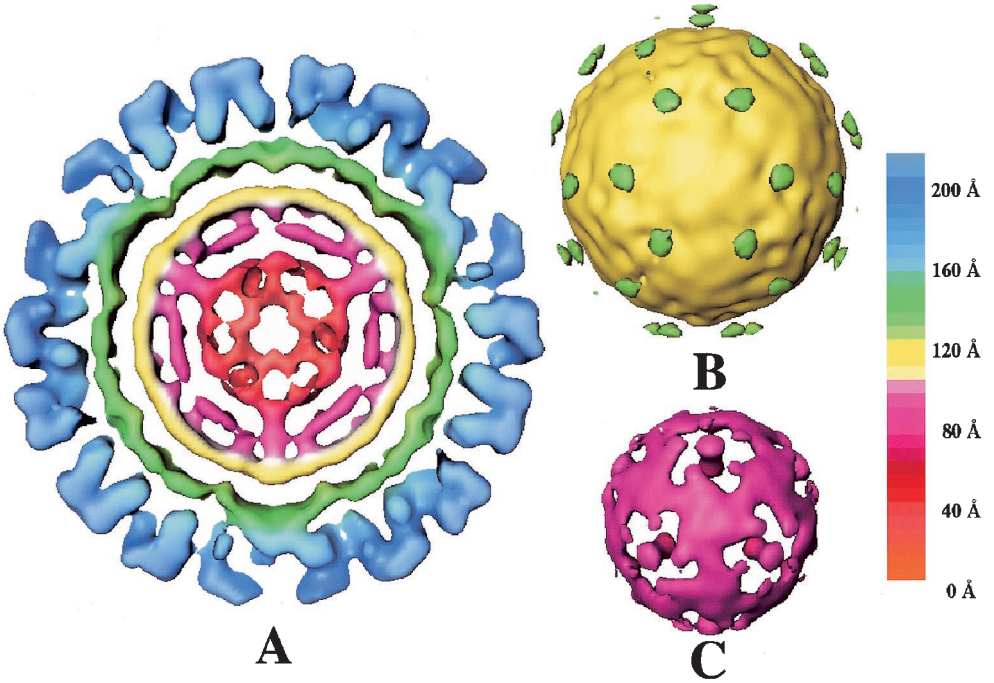

FIG. 5. Internal features in the SMSV4 virion structure. (A) Central equatorial section (20 Å in thickness) from SMSV4 map radially color coded according to the chart shown on the right. The P and S domain densities are shown in blue and green, respectively; the IS beneath the S-domain shell is shown in yellow. (B) Surface representation of IS and the weak densities that connect the IS with the S domain. (C) SMSV4 density map between the radii of 40 and 85 Å.

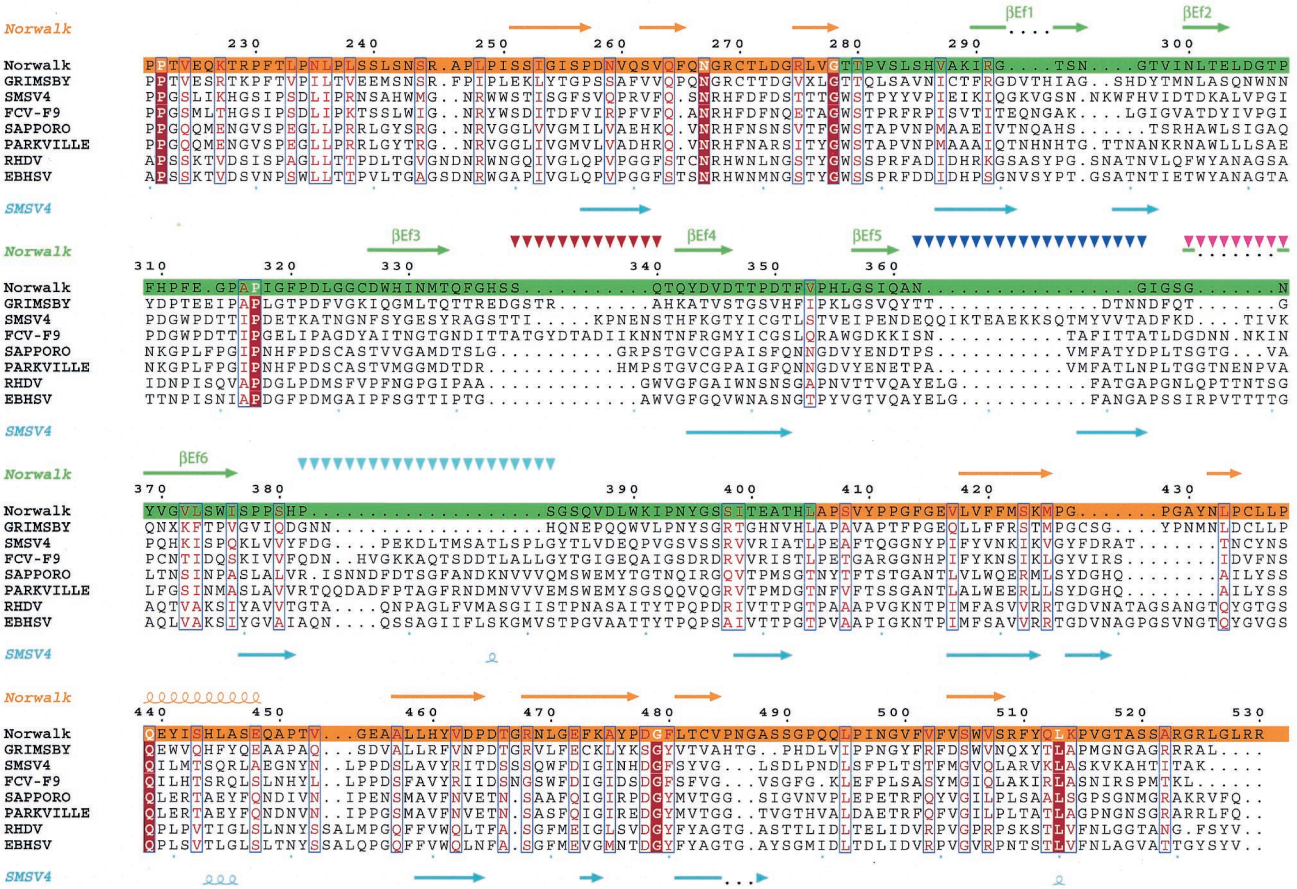

FIG. 6. Sequence alignment in the P domain, derived by comparing 30 calicivirus capsid protein sequences with the program CLUSTALW. Only eight calicivirus sequences (two from each genus), including those of NV, SMSV4, GrV, and PV, are shown. The secondary structural elements inferred from the rNV X-ray structure are shown above the sequences. As an example, the predicted secondary structure of SMSV4 is shown below. The numbers above the sequences correspond to the residue numbers in the NV sequence. Residues which are strictly conserved and moderately conserved are shown in red and pink, respectively. The regions corresponding to the P1 and P2 subdomains are highlighted in orange and green, respectively. Possible regions of insertion in SMSV4 are shown by inverted triangles.

towards the icosahedral threefold axis. As a control, rigid body refinement was first carried out with the rNV cryo-EM map, and the R factor dropped from 0.40 to 0.35. In the case of rGrV, a visual inspection indicated an overall good match of the rNV structure in the cryo-EM map, except for some density mismatches in the P2 region, whereas for the rPV and SMSV4 maps, it was clear from a visual inspection that only the rNV S domain matched well with the corresponding cryo-EM density map. The rigid body refinement, when applied to the rGrV density map, produced a final R factor of 0.46, and the final model, consistent with the visual inspection, did not show any significant variations in the relative orientations between different regions. The higher R factor was possibly due to density mismatches in the P2 region. However, in the case of rPV and SMSV4, the P1 domain was rotated about 30° from the rNV P1 coordinates. Thus, in both structures, the P1 subdomain exhibits a different orientation with respect to the S domain from that seen in the rNV structure. Unlike the P1 model, the fitted P2 model revealed no significant movement from the rNV structure; therefore, the relative orientation between the P1 and P2 subdomains is also different from that seen in the rNV structure. However, there was a significant amount of unaccounted extra density in the P2 region (Fig. 7). This extra density was likely due to the insertions seen in the sequence alignment (~45 residues for PV and ~50 residues for SMSV4) (Fig. 6). The R factors for both rPV and SMSV4 dropped from 0.55 to 0.46 after rigid body refinement.

DISCUSSION

Conserved structural features across different caliciviruses. The work presented in this paper, together with previous structural analyses of caliciviruses (44–46, 58), clearly demonstrates that the capsid architecture based on a T=3 icosahedral symmetry with 90 dimers is conserved across the family *Caliciviridae*. More importantly, these studies further indicate that, despite noticeable structural differences, the modular S-P1-P2 domain organization of the capsid protein, similar to that seen in the X-ray structure of rNV, is duplicated in all of the caliciviruses. In caliciviruses, the icosahedral capsid is formed from a single gene product. While common among plant viruses, virus capsids made of a single structural protein are unusual among animal viruses. Consequently, all of the functional entities required for capsid assembly, receptor recogni-

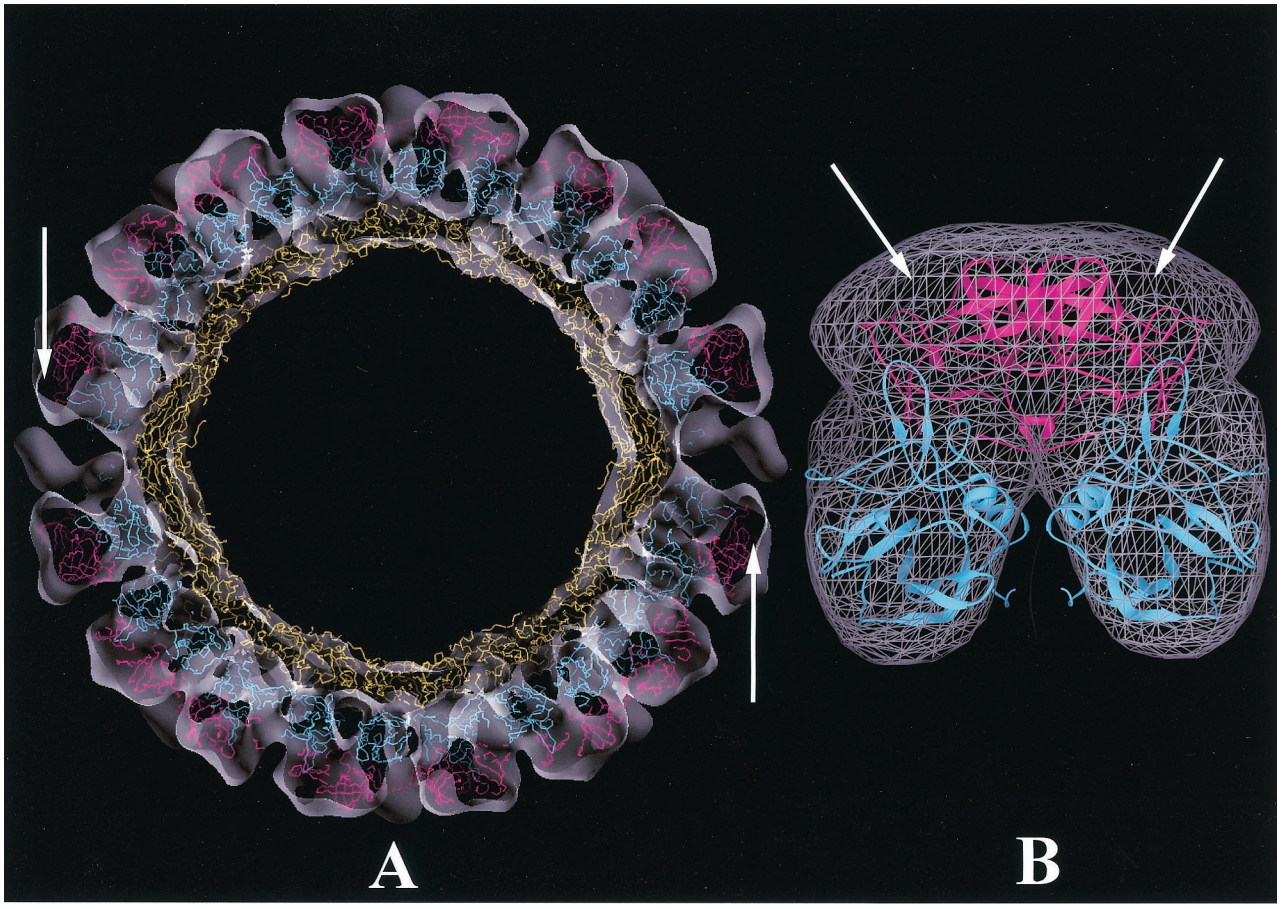

FIG. 7. Fitting of rNV capsid protein coordinates into the cryo-EM density map of SMSV4. (A) Central section viewed along the icosahedral twofold axis, with the rNV capsid structure fitted into the cryo-EM density map of SMSV4 shown as a semitransparent surface. The S, P1, and P2 domains of rNV, colored in yellow, cyan, and magenta, respectively, were each treated as a rigid body during fitting and refinement. For clarity, only the Cα backbone is shown. A reasonably good fitting is seen in the S and P1 regions. The arrows indicate some extra densities in the P2 region that are not occupied by the rNV coordinates. (B) Cryo-EM densities (wired cage) of the P regions of the SMSV4 CC dimer fitted with rNV coordinates shown in a ribbon representation following the same color scheme as for panel A. Extra densities in the P2 region are indicated by arrows.

tion, host specificity, strain diversity, and immunogenicity are encoded in a single structural protein. Perhaps the observed modular domain organization of the calicivirus capsid protein is necessitated by the requirement to integrate all of these properties into a single gene product. In their capsid architecture and capsid protein domain organization, caliciviruses resemble the plant tombusviruses, such as tomato bushy stunt virus (23) and turnip crinkle virus (24). However, the P domain in caliciviruses is significantly larger, with two subdomains that fold into a different tertiary structure.

The most conserved feature in the calicivirus structures examined thus far is the contiguous shell, which provides a platform for the protruding portions of the dimeric capsomeres. In the X-ray structure of rNV, this contiguous shell is formed by the closely interacting S domains of the 180 capsid protein subunits. This is the only domain that consistently fits well into the cryo-EM maps of the other caliciviruses examined. In rNV, the S domain is composed of residues 50 to 225, which fold into a typical eight-strand antiparallel β-barrel structure. In all of the caliciviruses, the residues in this region showed high conservation levels and similar secondary structural preferences. Based on the matching radial locations and the thickness of the contiguous shell, as seen by superimposing the radial density plots onto each other, it is likely that the S domain of the capsid proteins of all caliciviruses exhibits an eight-strand β-barrel fold. It is interesting that the radial disposition and also the thickness of the contiguous shell in caliciviruses match with those of other T=3 and P=3 icosahedral viruses in which the β-barrel motifs tile together to form an icosahedral shell (http://mmtsb.scripps.edu/viper/viper.html). Previous mutagenesis studies demonstrated that a capsid protein mutant of NV with only the S domain is sufficient for icosahedral particle assembly, suggesting that the role of the S domain is to provide a scaffold for icosahedral assembly (3).

Structural variations in the P domain. In contrast to the S domain, the P domains of different caliciviruses show substantial structural variations. As seen in the crystal structure of rNV, the P domain is linked to the S domain via a flexible hinge and is divided into P1 and P2 subdomains, which correspond to the leg and the top of the arch-like capsomere, respectively. The observed structural variations in the P domains of various caliciviruses are of two types. One of them regards

the relative orientation of the P domain with respect to the S domain, and the other regards the shape and size of the P2 subdomain. Our comparative analysis indicated that the changes in P-domain orientation were more pronounced between the viruses from different genera than between those within the same genus. The size and shape of the P2 subdomain, however, appeared to be characteristic of each individual calicivirus.

The P1 subdomain. The variations in P-domain orientation are likely facilitated by the hinge region. Changes in the P-domain orientation result in the alteration of interactions between the dimeric subunits. In all of the caliciviruses, the P domain is exclusively involved in dimeric interactions. In both the rNV and rGrV structures, both the P1 and P2 subdomains are involved in intradimeric interactions. In contrast, for the sapoviruses and vesiviruses examined, our studies suggest that only the P2 subdomain participates in intradimeric interactions, whereas the P1 subdomain is involved in interdimeric interactions, as is evident from the structures of rPV and SMSV4, in which the density that emanates immediately from the S domain, corresponding to the P1 subdomain, is displaced significantly from its dimeric counterpart compared to what is seen in the rNV and rGrV structures. This observation further suggests that the P2 subdomain has to undergo a compensatory change in its orientation with respect to the P1 subdomain to maintain the dimeric interactions across the local and strict twofold axes. Indeed, a strictly conserved glycine (residue 278 in the NV capsid protein) located at the P1-P2 connecting region (Fig. 6) may facilitate such changes in the relative orientation between the P1 and P2 subdomains. Thus, in addition to the flexibility between the S domain and the P1 subdomain, our studies indicate that caliciviruses have flexibility between the P1 and P2 subdomains. Such multiple points of flexibility are reminiscent of antibody structures, in which Fc and Fab arms are linked by a flexible hinge, with additional flexibility between the constant and variable domains in each Fab arm (10). It is possible that, like antibodies, caliciviruses exploit the two points of flexibility to achieve more strain diversity. Like the role of the constant region of Fab arms, a possible role of the P1 subdomain, which is moderately conserved between the calicivirus sequences, is to provide a platform to appropriately orient the hypervariable P2 subdomain.

Is the tertiary structure of the P1 subdomain conserved in the caliciviruses? Several observations suggest that the overall tertiary structure of this subdomain is likely to be maintained in all caliciviruses. First, the P1 subdomain exhibits moderate conservation in its amino acid sequence. Second, the secondary structure of this subdomain, including an α-helix, also appears to be conserved among different caliciviruses. Third, despite changes in the orientation of this subdomain with respect to the S domain, the X-ray structure of the P1 subdomain of rNV can be fitted, as a rigid body, reasonably well into the corresponding regions in the cryo-EM maps of rGrV, rPV, and SMSV4.

The P2 subdomain. According to the X-ray structure of the rNV capsid, the distally located P2 subdomain can be considered a large insertion in the P1 subdomain (44). Multiple sequence alignments have indicated that this subdomain is the most variable region (17, 29). In an alignment of calicivirus sequences with respect to the rNV sequence, a large number of insertions were seen in the SMSV4 and PV sequences and fewer and less prominent insertions were seen in the GrV sequence. The observed structural variations in size and shape appeared to correlate well with the sequence variations. The crystallographic structure of rNV indicates that the P2 subdomain folds into a structure similar to that seen in RNA binding domain 2 of the elongation factor Tu. Compared to NV, GrV contains a similar number of residues in the P2 subdomain. In addition, its secondary structure preference appears to be similar to that of NV and the size and the shape of this domain match, taking into consideration the sequence variations, those of the P2 subdomain in NV. Therefore, it is likely that a fold similar to the one in NV is present in the P2 subdomain of GrV. However, in the case of SMSV4 and PV, it is difficult to predict whether a similar folding is conserved in their respective P2 subdomains because of the large number of insertions (totaling ~45 residues for PV and ~50 residues for SMSV4).

Several lines of evidence suggest that the hypervariable P2 subdomain contains determinants for cell binding, antigenicity, and host specificity (21, 25, 39, 58, 59, 62). Based on the X-ray structure of the rNV capsid, it is hypothesized that the P2 subdomain functions as a replaceable module to confer strain diversity in caliciviruses. Although our structural studies support this idea, further X-ray crystallographic studies of representative caliciviruses from different genera will be necessary to substantiate this notion and to understand the role of this domain in calicivirus strain divergence and biology.

Structural similarities between sapoviruses and animal caliciviruses. One of the interesting observations from our structural studies is that the capsid structure of rPV, despite being a human calicivirus of the genus *Sapovirus*, is more similar to SMSV4, an animal calicivirus in the genus *Vesivirus*, than to either rNV or rGrV, which are both human pathogens of the genus *Norovirus*. Such an observation, which is indeed in agreement with previous negative stain studies (17, 37) and sequence comparison results (38), indicates a closer relationship between sapoviruses and animal caliciviruses. The striking similarity between sapoviruses and animal caliciviruses is also suggestive of possible zoonoses of caliciviruses emerging from marine and animal reservoirs. The potential existence of animal reservoirs and the possibility of interspecies transmission are also suggested by the phylogenetic relatedness of a porcine calicivirus within the genus *Sapovirus*.

Inner shell and genome packaging. The 3D structures of a primate calicivirus (45) and SMSV4, both of which are authentic virions with intact genomes, reveal distinct internal features that are not seen in those of the recombinant human calicivirus capsids. In addition to the arch-like protrusions and icosahedral shell seen in the empty capsid structure, these authentic virions exhibit an additional shell of significant density, referred to as the IS, immediately underneath the contiguous shell formed by the S domains. Although structures of authentic human caliciviruses are not available, it is likely that a similar internal structural organization is present in human calicivirus virions.

The genomes of caliciviruses range from 7.4 to 8.3 kb, with an average molecular mass of about 2.65×10^6 Da. Given this genomic molecular weight and assuming a partial specific volume of dry RNA of 0.55 cm^3/g, the minimum radius required to package the calicivirus genome is 84 Å. Among different

single-stranded RNA viruses, the genomic size of picornaviruses (2.55×10^6 Da) compares well with that of caliciviruses. In picornaviruses, the calculated density for the RNA genome is 0.59 Da/Å^3 (48). If the calicivirus genome is similarly packaged, a spherical container with a radius of 102 Å is needed. Thus, the genomic RNA could significantly contribute to the IS density, which extends from radii of 85 to 105 Å.

In addition to the genomic RNA, we cannot rule out the possibility that the N-terminal residues of the capsid protein also contribute to the density in the inner shell. In the X-ray structure of rNV, the N-terminal 28 residues in the A and C subunits and the N-terminal 9 residues in the B subunit are disordered (44). In the presence of RNA, these N-terminal residues might form stable structures. The additional ordering of the N-terminal arm of the capsid protein in the presence of the genome has been observed by comparative crystallographic analyses of the empty (32) and full particles (31) of tymoviruses. In both caliciviruses and tymoviruses, the capsid protein does not contain a basic N-terminal arm, suggesting that such an ordering may require some specific interactions between the N-terminal residues and the genomic RNA. In the 3D structure of SMSV4, 60 densities that connect the inner shell with the shell formed by the S domains are consistently seen in independent reconstructions. It is possible that they represent portions of the RNA genome and/or an ordered N-terminal arm connecting the two shells.

In summary, our comparative structural analysis of caliciviruses indicates that, despite their overall similarity with respect to the icosahedral and subunit domain organization, these viruses exhibit significant structural variations, particularly in the P domain. The unique modular organization of the calicivirus capsid protein subunit, consisting of an N-terminal arm, a highly conserved S domain, a moderately conserved P1 subdomain, and a hypervariable P2 subdomain, may have evolved to integrate various capsid-associated functions, such as assembly, receptor recognition, host specificity, and immune evasion, in a single structural protein. Such a modular organization with multiple flexible regions is reminiscent of the structure of antibodies and is perhaps used to achieve more strain diversity. Further high-resolution structural studies are necessary to examine if the tertiary structure in the P domain is conserved and to understand the role of the P2 subdomain in host interactions and its possible role as a replaceable module in conferring strain diversity.

ACKNOWLEDGMENTS

This work was supported by grants from the NIH (RO1AI38036 to M.K.E. and B.V.V.P.) and the R. A. Welch Foundation (B.V.V.P.). A.M.H. was supported by grant CA-09197 from the NIH.

REFERENCES

1. **Anonymous.** 1994. The CCP4 suite: programs for protein crystallography. Acta Crystallogr. D **50:**760–763.
2. **Belliot, G., J. S. Noel, J. F. Li, Y. Seto, C. D. Humphrey, T. Ando, R. I. Glass, and S. S. Monroe.** 2001. Characterization of capsid genes, expressed in the baculovirus system, of three new genetically distinct strains of "Norwalk-like viruses." J. Clin. Microbiol. **39:**4288–4295.
3. **Bertolotti-Ciarlet, A., L. J. White, R. Chen, B. V. Prasad, and M. K. Estes.** 2002. Structural requirements for the assembly of Norwalk virus-like particles. J. Virol. **76:**4044–4055.
4. **Brünger, A. T.** 1993. XPLOR manual,version 3.1. Yale University, New Haven, Conn.
5. **Carter, M. J., I. D. Milton, P. C. Turner, J. Meanger, M. Bennett, and R. M. Gaskell.** 1992. Identification and sequence determination of the capsid protein gene of feline calicivirus. Arch. Virol. **122:**223–235.
6. **Clarke, I. N., and P. R. Lambden.** 1997. Viral zoonoses and food of animal origin: caliciviruses and human disease. Arch. Virol. **13**(Suppl.)**:**141–152.
7. **Crowther, R. A.** 1971. Procedures for three-dimensional reconstruction of spherical viruses by Fourier synthesis from electron micrographs. Phil. Trans. R. Soc. Lond. B **261:**221–230.
8. **Crowther, R. A., D. J. DeRosier, and A. Klug.** 1970. The reconstruction of a three-dimensional structure from projections and its applications to electron microscopy. Proc. R. Soc. Lond. A **317:**319–340.
9. **Dastjerdi, A. M., J. Green, C. I. Gallimore, D. W. Brown, and J. C. Bridger.** 1999. The bovine Newbury agent-2 is genetically more closely related to human SRSVs than to animal caliciviruses. Virology **254:**1–5.
10. **Davies, D. R., E. A. Padlan, and S. Sheriff.** 1990. Antibody-antigen complexes. Annu. Rev. Biochem. **59:**439–473.
11. **Dingle, K. E., P. R. Lambden, E. O. Caul, and I. N. Clarke.** 1995. Human enteric Caliciviridae: the complete genome sequence and expression of virus-like particles from a genetic group II small round structured virus. J. Gen. Virol. **76:**2349–2355.
12. **Dubochet, J., M. Adrian, J. J. Chang, J. C. Homo, J. Lepault, A. W. McDowall, and P. Schultz.** 1988. Cryo-electron microscopy of vitrified specimens. Q. Rev. Biophys. **21:**129–228.
13. **Estes, M. K., and M. E. Hardy.** 1995. Norwalk virus and other enteric caliciviruses, p. 1009–1034. *In* M. Blaser, P. Smith, J. Ravdin, H. B. Greenberg, and R. Guerrant (ed.), Infections of the gastrointestinal tract. Raven Press, New York, N.Y.
14. **Fankhauser, R. L., J. S. Noel, S. S. Monroe, T. Ando, and R. I. Glass.** 1998. Molecular epidemiology of "Norwalk-like viruses" in outbreaks of gastroenteritis in the United States. J. Infect. Dis. **178:**1571–1578.
15. **Fretz, M., and F. L. Schaffer.** 1978. Calicivirus proteins in infected cells: evidence for a capsid polypeptide precursor. Virology **89:**318–321.
16. **Green, K. Y., T. Ando, M. S. Balayan, T. Berke, I. N. Clarke, M. K. Estes, D. O. Matson, S. Nakata, J. D. Neill, M. J. Studdert, and H. J. Thiel.** 2000. Taxonomy of the caliciviruses. J. Infect. Dis. **181**(Suppl. 2)**:**S322–S330.
17. **Green, K. Y., R. M. Chanock, and A. Z. Kapikian.** 2001. Human caliciviruses, p. 841–874. *In* D. M. Knipe et al. (ed.), Fields virology. Lippincott Williams & Wilkins, Philadelphia, Pa.
18. **Green, K. Y., A. Z. Kapikian, J. Valdesuso, S. Sosnovtsev, J. J. Treanor, and J. F. Lew.** 1997. Expression and self-assembly of recombinant capsid protein from the antigenically distinct Hawaii human calicivirus. J. Clin. Microbiol. **35:**1909–1914.
19. **Green, K. Y., A. Mory, M. H. Fogg, A. Weisberg, G. Belliot, M. Wagner, T. Mitra, E. Ehrenfeld, C. E. Cameron, and S. V. Sosnovtsev.** 2002. Isolation of enzymatically active replication complexes from feline calicivirus-infected cells. J. Virol. **76:**8582–8595.
20. **Guo, M., K. O. Chang, M. E. Hardy, Q. Zhang, A. V. Parwani, and L. J. Saif.** 1999. Molecular characterization of a porcine enteric calicivirus genetically related to Sapporo-like human caliciviruses. J. Virol. **73:**9625–9631.
21. **Guo, M., J. Hayes, K. O. Cho, A. V. Parwani, L. M. Lucas, and L. J. Saif.** 2001. Comparative pathogenesis of tissue culture-adapted and wild-type Cowden porcine enteric calicivirus (PEC) in gnotobiotic pigs and induction of diarrhea by intravenous inoculation of wild-type PEC. J. Virol. **75:**9239–9251.
22. **Hale, A. D., S. E. Crawford, M. Ciarlet, J. Green, C. Gallimore, D. W. Brown, X. Jiang, and M. K. Estes.** 1999. Expression and self-assembly of Grimsby virus: antigenic distinction from Norwalk and Mexico viruses. Clin. Diagn. Lab. Immunol. **6:**142–145.
23. **Harrison, S. C., A. J. Olson, C. E. Schutt, F. K. Winkler, and G. Bricogne.** 1978. Tomato bushy stunt virus at 2.9 A resolution. Nature **276:**368–373.
24. **Hogle, J. M., A. Maeda, and S. C. Harrison.** 1986. Structure and assembly of turnip crinkle virus. I. X-ray crystallographic structure analysis at 3.2 A resolution. J. Mol. Biol. **191:**625–638.
25. **Huston, A. M., R. L. Atmar, D. M. Marcus, and M. K. Estes.** 2003. Norwalk virus-like particle hemagglutination by binding to H histo-blood group antigens. J. Virol. **77:**405–415.
26. **Jiang, X., D. O. Matson, G. M. Ruiz-Palacios, J. Hu, J. Treanor, and L. K. Pickering.** 1995. Expression, self-assembly, and antigenicity of a snow mountain agent-like calicivirus capsid protein. J. Clin. Microbiol. **33:**1452–1455.
27. **Jiang, X., M. Wang, D. Y. Graham, and M. K. Estes.** 1992. Expression, self-assembly, and antigenicity of the Norwalk virus capsid protein. J. Virol. **66:**6527–6532.
28. **Jones, T. A., J. Y. Zou, S. W. Xowan, and M. Kjeldgaard.** 1991. Improved methods for building protein models in electron density maps and the location of errors in these models. Acta Crystallogr. A **47:**392–400.
29. **Kapikian, A. Z., M. K. Estes, and R. M. Chanock.** 1996. Norwalk group of viruses, p. 783–810. *In* B. N. Fields, D. M. Knipe, and P. M. Howley (ed.), Fields virology, 3rd ed. Lippincott-Raven Publishers, Philadelphia, Pa.
30. **Kobayashi, S., K. Sakae, Y. Suzuki, H. Ishiko, K. Kamata, K. Suzuki, K. Natori, T. Miyamura, and N. Takeda.** 2000. Expression of recombinant capsid proteins of chitta virus, a genogroup II Norwalk virus, and development of an ELISA to detect the viral antigen. Microbiol. Immunol. **44:**687–693.

31. **Krishna, S. S., C. N. Hiremath, S. K. Munshi, D. Prahadeeswaran, M. Sastri, H. S. Savithri, and M. R. Murthy.** 1999. Three-dimensional structure of Physalis mottle virus: implications for the viral assembly. J. Mol. Biol. **289:**919–934.
32. **Krishna, S. S., M. Sastri, H. S. Savithri, and M. R. Murthy.** 2001. Structural studies on the empty capsids of Physalis mottle virus. J. Mol. Biol. **307:**1035–1047.
33. **Lawton, J. A., and B. V. V. Prasad.** 1996. Automated software package for icosahedral virus reconstruction. J. Struct. Biol. **116:**209–215.
34. **Leite, J. P., T. Ando, J. S. Noel, B. Jiang, C. D. Humphrey, J. F. Lew, K. Y. Green, R. I. Glass, and S. S. Monroe.** 1996. Characterization of Toronto virus capsid protein expressed in baculovirus. Arch. Virol. **141:**865–875.
35. **Liu, B. L., P. R. Lambden, H. Gunther, P. Otto, M. Elschner, and I. N. Clarke.** 1999. Molecular characterization of a bovine enteric calicivirus: relationship to the Norwalk-like viruses. J. Virol. **73:**819–825.
36. **Love, D. N., and M. Sabine.** 1975. Electron microscopic observation of feline kidney cells infected with a feline calicivirus. Arch. Virol. **48:**213–228.
37. **Madeley, C. R., and B. P. Cosgrove.** 1976. Letter: caliciviruses in man. Lancet **i:**199–200.
38. **Matson, D. O., W. M. Zhong, S. Nakata, K. Numata, X. Jiang, L. K. Pickering, S. Chiba, and M. K. Estes.** 1995. Molecular characterization of a human calicivirus with sequence relationships closer to animal caliciviruses than other known human caliciviruses. J. Med. Virol. **45:**215–222.
39. **Matsuura, Y., Y. Tohya, M. Mochizuki, K. Takase, and T. Sugimura.** 2001. Identification of conformational neutralizing epitopes on the capsid protein of canine calicivirus. J. Gen. Virol. **82:**1695–1702.
40. **Neill, J. D.** 1992. Nucleotide sequence of the capsid protein gene of two serotypes of San Miguel sea lion virus: identification of conserved and nonconserved amino acid sequences among calicivirus capsid proteins. Virus Res. **24:**211–222.
41. **Neill, J. D., and W. L. Mengeling.** 1988. Further characterization of the virus-specific RNAs in feline calicivirus infected cells. Virus Res. **11:**59–72.
42. **Noel, J. S., B. L. Liu, C. D. Humphrey, E. M. Rodriguez, P. R. Lambden, I. N. Clarke, D. M. Dwyer, T. Ando, R. I. Glass, and S. S. Monroe.** 1997. Parkville virus: a novel genetic variant of human calicivirus in the Sapporo virus clade, associated with an outbreak of gastroenteritis in adults. J. Med. Virol. **52:**173–178.
43. **Numata, K., M. E. Hardy, S. Nakata, S. Chiba, and M. K. Estes.** 1997. Molecular characterization of morphologically typical human calicivirus Sapporo. Arch. Virol. **142:**1537–1552.
44. **Prasad, B. V., M. E. Hardy, T. Dokland, J. Bella, M. G. Rossmann, and M. K. Estes.** 1999. X-ray crystallographic structure of the Norwalk virus capsid. Science **286:**287–290.
45. **Prasad, B. V., D. O. Matson, and A. W. Smith.** 1994. Three-dimensional structure of calicivirus. J. Mol. Biol. **240:**256–264.
46. **Prasad, B. V., R. Rothnagel, X. Jiang, and M. K. Estes.** 1994. Three-dimensional structure of baculovirus-expressed Norwalk virus capsids. J. Virol. **68:**5117–5125.
47. **Rossmann, M. G., and J. E. Johnson.** 1989. Icosahedral RNA virus structure. Annu. Rev. Biochem. **58:**533–573.
48. **Schneemann, A., V. Reddy, and J. E. Johnson.** 1998. The structure and function of nodavirus particles: a paradigm for understanding chemical biology. Adv. Virus Res. **50:**381–446.
49. **Smiley, J. R., K. O. Chang, J. Hayes, J. Vinje, and L. J. Saif.** 2002. Characterization of an enteropathogenic bovine calicivirus representing a potentially new calicivirus genus. J. Virol. **76:**10089–10098.
50. **Smith, A. W., T. G. Akers, S. H. Madin, and N. A. Vedros.** 1973. San Miguel sea lion virus isolation, preliminary characterization and relationship to vesicular exanthema of swine virus. Nature **244:**108–110.
51. **Smith, A. W., E. S. Berry, D. E. Skilling, J. E. Barlough, S. E. Poet, T. Berke, J. Mead, and D. O. Matson.** 1998. In vitro isolation and characterization of a calicivirus causing a vesicular disease of the hands and feet. Clin. Infect. Dis. **26:**434–439.
52. **Smith, A. W., C. M. Prato, and D. E. Skilling.** 1977. Characterization of two new serotypes of San Miguel sea lion virus. Intervirology **8:**30–36.
53. **Smith, A. W., D. E. Skilling, N. Cherry, J. H. Mead, and D. O. Matson.** 1998. Calicivirus emergence from ocean reservoirs: zoonotic and interspecies movements. Emerg. Infect. Dis. **4:**13–20.
54. **Smith, A. W., D. E. Skilling, P. K. Ensley, K. Benirschke, and T. L. Lester.** 1983. Calicivirus isolation and persistence in a pygmy chimpanzee (Pan paniscus). Science **221:**79–81.
55. **Smith, A. W., D. E. Skilling, and A. B. Latham.** 1981. Isolation and identification of five new serotypes of calicivirus from marine mammals. Am. J. Vet Res. **42:**693–694.
56. **Sosnovtsev, S. V., S. A. Sosnovtseva, and K. Y. Green.** 1998. Cleavage of the feline calicivirus capsid precursor is mediated by a virus-encoded proteinase. J. Virol. **72:**3051–3059.
57. **Sugieda, M., H. Nagaoka, Y. Kakishima, T. Ohshita, S. Nakamura, and S. Nakajima.** 1998. Detection of Norwalk-like virus genes in the caecum contents of pigs. Arch. Virol. **143:**1215–1221.
58. **Thouvenin, E., S. Laurent, M. F. Madelaine, D. Rasschaert, J. F. Vautherot, and E. A. Hewat.** 1997. Bivalent binding of a neutralising antibody to a calicivirus involves the torsional flexibility of the antibody hinge. J. Mol. Biol. **270:**238–246.
59. **Tohya, Y., K. Masuoka, E. Takahashi, and T. Mikami.** 1991. Neutralizing epitopes of feline calicivirus. Arch. Virol. **117:**173–181.
60. **van Der Poel, W. H., J. Vinje, R. van Der Heide, M. I. Herrera, A. Vivo, and M. P. Koopmans.** 2000. Norwalk-like calicivirus genes in farm animals. Emerg. Infect. Dis. **6:**36–41.
61. **van Heel, M.** 1987. Similarity measures between images. Ultramicroscopy **21:**95–100.
62. **White, L. J., J. M. Ball, M. E. Hardy, T. N. Tanaka, N. Kitamoto, and M. K. Estes.** 1996. Attachment and entry of recombinant Norwalk virus capsids to cultured human and animal cell lines. J. Virol. **70:**6589–6597.
63. **Zhou, Z. H., B. V. Prasad, J. Jakana, F. J. Rixon, and W. Chiu.** 1994. Protein subunit structures in the herpes simplex virus A-capsid determined from 400 kV spot-scan electron cryomicroscopy. J. Mol. Biol. **242:**456–469.